BOREAL ENVIRONMENT RESEARCH 21: 207–220
ISSN 1239-6095 (print) ISSN 1797-2469 (online)

Helsinki 23 May 2016

Measuring atmospheric ion bursts and their dynamics using mass spectrometry

Heikki Junninen[1], Jonathan Duplissy[1,2], Mikael Ehn[1], Mikko Sipilä[1], Juha Kangasluoma[1], Alessandro Franchin[1], Tuukka Petäjä[1], Hanna E. Manninen[1], Veli-Matti Kerminen[1], Douglas Worsnop[1,3] and Markku Kulmala[1]

[1)] *Department of Physics, P.O. Box 64, FI-00014 University of Helsinki, Finland*
[2)] *Helsinki Institute of Physics, P.O. Box 64, FI-00014 University of Helsinki, Finland*
[3)] *Aerodyne Research Inc., 45 Manning Road Billerica, MA 01821-3976, USA*

Received 3 Dec. 2015, final version received 31 Mar. 2016, accepted 4 Apr. 2016

Junninen H., Duplissy J., Ehn M., Sipilä M., Kangasluoma J., Franchin A., Petäjä T., Manninen H.E., Kerminen V.-M., Worsnop D. & Kulmala M. 2016: Measuring atmospheric ion bursts and their dynamics using mass spectrometry. *Boreal Env. Res.* 21: 207–220.

Atmospheric ions are produced after a cascade of reactions starting from initial ionization by high energetic radiation. Such ionization bursts generate ions that rapidly react and generate a suite of ion products. Primary ions are in the atmosphere originate from radioactive decay, gamma radiation from the soil or cosmic ray events. In this work, we modified an existing instrumentation and developed a novel setup for detecting ion bursts. The setup consists of a continuous flow ionization chamber coupled to Atmospheric Pressure interface Time-Of-Flight (APi-TOF) mass spectrometer. The APi-TOF sampling rate was set to 100 Hz in order to detect individual ion bursts from ionization events. Besides counting the individual ionization events, the developed setup is able to follow the rapidly changing chemical composition of ions during ion burst cascade. The setup can give us insights into the primary ionization mechanisms and their importance in atmospheric ion and aerosol dynamics.

Introduction

Atmospheric ions are fundamental to atmospheric electricity (Israël 1970, Singh *et al*. 2011), in addition to which they affect the chemical composition of the atmospheric, dynamics of atmospheric aerosol particles and cloud properties (Harrison and Ambaum 2008, Calisto *et al*. 2011, Larin 2011, Harrison *et al*. 2015, Mironova *et al*. 2015). Ions are known to enhance nucleation rates under conditions relevant to the ambient atmosphere (e.g. Raes *et al*. 1986, Kirkby *et al*. 2011, Duplissy *et al*. 2016), but their overall effect on atmospheric new-particle formation and subsequent cloud condensation nuclei production has remained poorly quantified (e.g. Iida *et al*. 2006, Gagne *et al*. 2008, Manninen *et al*. 2010, Hirsikko *et al*. 2011, Yu and Lee 2012, Kontkanen *et al*. 2013, Kulmala *et al*. 2013). Ions are central to the proposed connection between solar activity, cosmic rays, clouds and climate (Dickinson 1975, Svensmark 1998), a topic which has been investigated extensively using laboratory experiments (Kirkby *et al*.

Editor in charge of this article: Hannele Korhonen

2011), atmospheric observations (e.g. Kulmala *et al*. 2010, Laken *et al*. 2012, Voiculescu and Usoskin 2012) and large-scale model simulations (e.g. Pierce and Adams 2009, Snow-Kropla *et al*. 2011, Kazil *et al*. 2012).

Air ions are produced by galactic cosmic rays (GCRs), as well as by radon decay and gamma radiation originating from the soil (Israël 1970, Bazilevskaya *et al*. 2008). Terrestrial sources are usually more important than GCRs for ion production taking place within a continental planetary boundary layer, whereas in the free troposphere the GCRs play the dominant role (e.g. Kazil and Lovejoy 2004, Williams *et al*. 2011, Zhang, *et al*. 2011). After their formation in the atmosphere, the primary ions (N_2^+, O_2^+ and e^-) are rapidly converted into secondary molecular ions (Arnold 2006, Larin 2011), and then either neutralized by ion–ion recombination or attached to aerosol particles and removed from the relevant mobility regime (Israël 1970). The final composition of ambient ions is defined by the composition of neutral gases and their proton and electron affinities (Eisele 1988, Smith and Spanel 1996, Ehn *et al*. 2010).

Cosmic rays are high-energy particles originating mostly from outside our solar system and even outside the Milky Way galaxy. Most of them are positively charged nuclei of hydrogen (89%) or helium (10%), the rest (about 1%) being made of heavier elements (Singh *et al*. 2011). The energy range of cosmic rays is 10^9–10^{21} eV (Singh *et al*. 2011). When entering Earth's atmosphere, the cosmic rays form secondary particles called air showers, in addition to which they ionize matter. In this way, the cosmic ray leaves a track of ions until it collides with a nucleus of molecule and gets terminated, as a result of which new secondary ionizing particles will be formed. On average, the cosmic rays produce one ion–electron pair per 35 eV of deposited energy (Porter *et al*. 1976).

Detailed investigation of the dynamics and chemistry of atmospheric ionization has been very difficult because of instrumental limitations. The earliest instruments capable of detecting ionizing radiation and observing the ion bursts are dated back to 1899 when Wilson constructed a cloud chamber and was able to observe condensation of vapours onto ions produced by radiation under supersaturated conditions (Wilson 1899). His work set the basis for high energy physics (Das Gupta and Ghosh 1946) and initiated the development towards modern aerosol and ion instruments (Flagan 1998, McMurry 2000). After the initial work of Wilson, the techniques on mobility classification and detection of ions have been refined (e.g. Tammet *et al*. 2002, Iida *et al*. 2006, Mirme *et al*. 2007, Manninen *et al*. 2009a, 2009b). The global *in-situ* ion observations were put into perspective in terms of their spatio-temporal variability and their role in the aerosol formation by Hirsikko *et al*. (2011). Although the response time of air ion instruments can be rapid (in order of seconds) (e.g. Lee *et al*. 2013, Mirme and Mirme 2013, Noe *et al*. 2016), typically the results are presented in minute-to-hour time resolution (Vana *et al*. 2008, Mirme *et al*. 2010, Ehn *et al*. 2011, Vana *et al*. 2016).

In this paper, we describe a new method for direct measurement of atmospheric ion bursts produced by cosmic rays, radioactive decay or gamma radiation. The method makes it possible to monitor individual ionization events during ion bursts and to measure the rapidly changing chemical composition of the ions associated with such bursts. The resulting information will be valuable for atmospheric scientists in exploring the effect of the ions on microphysical atmospheric processes and consequent on effects on climate in Earth's system.

Material and methods

Experimental setup

The laboratory setup for detecting ion bursts consists of a continuous flow ionization chamber for capturing ion bursts and a mass spectrometer for detecting the frequency and composition of the resulting ion plumes. The mass spectrometer used was an Atmospheric Pressure interface Time-Of-Flight mass spectrometer, APi-TOF (Tofwerk AG & Aerodyne Research Inc.; *see* Junninen *et al*. 2010). The instrument consists of two main parts: an APi interface that transfers ions from the atmospheric pressure to vacuum and a mass spectrometer that determines the mass-to-charge ratios of the ions. APi

has three differentially-pumped chambers, with two quadrupoles and ion lenses to focus and transport the ions. Once the ions arrive at the time-of-flight chamber of the mass spectrometer, they are accelerated orthogonally to their initial flight path. This acceleration process is called an extraction, and it is repeated at a frequency of around 10–12 kHz depending on the desired mass range. The ions are separated based on their flight time, which depends on the mass-to-charge ratio, and detected using a multi-channel plate (MCP) with intervals of 40–80 ps. The mass spectrometer has a mass resolving power of 3000–6000 Th/Th and mass accuracy better than 20 ppm (0.002%) (Junninen *et al*. 2010). The unit Thomson (Th) used here is equal to 1 u/e, where u is unified atomic mass unit and e is the elementary charge, i.e. the electric charge unit in the atomic unit system. The instrument is equipped with a reflector that reduces the physical dimensions of the instrument and improves mass resolving power both by adding length to flight path and by focusing the ions.

In the measurements discussed here, the mass spectrometer was set to measure the masses up to 2000 Th. No ionization source, except for the natural radiation, was used. The transmission of ions thorough the mass spectrometer was about 3% at 200 Th and 0.5% at 1000 Th. Different from earlier studies, the mass spectrometer was set to save spectra at a frequency of 100 Hz instead of the typical rate of ~1 Hz. This was done in order to capture the short ionization events and separate them from the background ion signals.

The continuous-flow ionization chamber was a tube with a length of 40 cm and internal diameter of 4 cm. The sample air (in this experiment indoor air) was taken through a High Efficiency Particulate Air (HEPA, Pall Corporation PN12144) filter and the other end of the ionization chamber was attached directly to the inlet of the mass spectrometer with connections to the flow control unit (Fig. 1). Three different flow rates through the chamber were used (2.8, 8.8 and 16.8 l min^{-1}), all of which were well within the laminar flow regime (Reynolds numbers of 98, 308 and 589, respectively, in the ionization chamber). If we assume that the ionization event happens just inside the flow ionization chamber entrance and take into account the flow rates, the resulting plug flow residence times are 15.1, 3.8 and 1.9 s, respectively.

Data handling

In order to achieve a high time-resolution for the ion burst measurements, we modified the data acquisition of the mass spectrometer. The typical acquisition method, where the whole mass spectrum is saved in every acquisition step, was changed to a so-called event-list saving method. In this saving mode, only individual events of ion detection are recorded, accompanied with their time of occurrence. The mass spectrum is then constructed in retrospect. This gives great advantages: First, the memory requirements are much smaller (but only in the cases, where total amount of signal counts are low, like here). Second, the reconstruction of mass spectrum can now be done in a completely new way: we are not constrained by the time interval of the acquisition, but instead, we can apply different criteria for co-adding the signal. As an example, if we need a measurement point every one second, traditionally we would need to co-add all the signal during the 1-s acquisition period (Fig. 2a), but now we can include or exclude data that have, for example, too few counts during the 10-ms acquisition period (Fig. 2b). The final time series is still provided with the 1-s time resolution, but its information content is different. Third, different ways of reconstructing the mass spectra are not exclusive and acquisition data can be processed in multiple ways in parallel in order to get more information.

When sampling at 100 Hz, one acquisition period is 10 ms. The terminology used in this work is as follows: data from the primary data acquisition period is called a raw spectrum, whereas a reconstructed spectrum is called a cumulative spectrum.

Data processing forms a process chain with multiple consecutive steps: (1) calculating total ion counts (TIC) in each raw spectrum, (2) finding data corresponding to the ion bursts from the time series of TIC signal, (3) co-adding all the mass spectra signal corresponding to the found ion burst, so that we get a mass spectrum

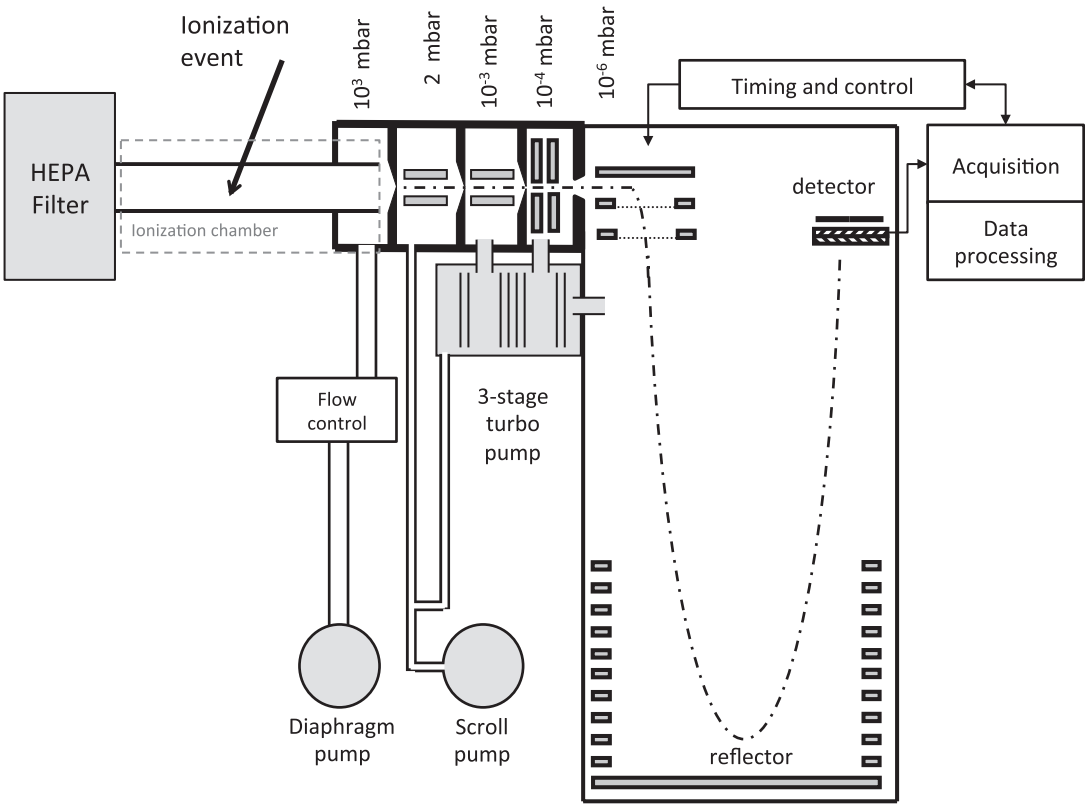

Fig. 1. Schematic of instrumentations used for measuring chemical composition of ion bursts.

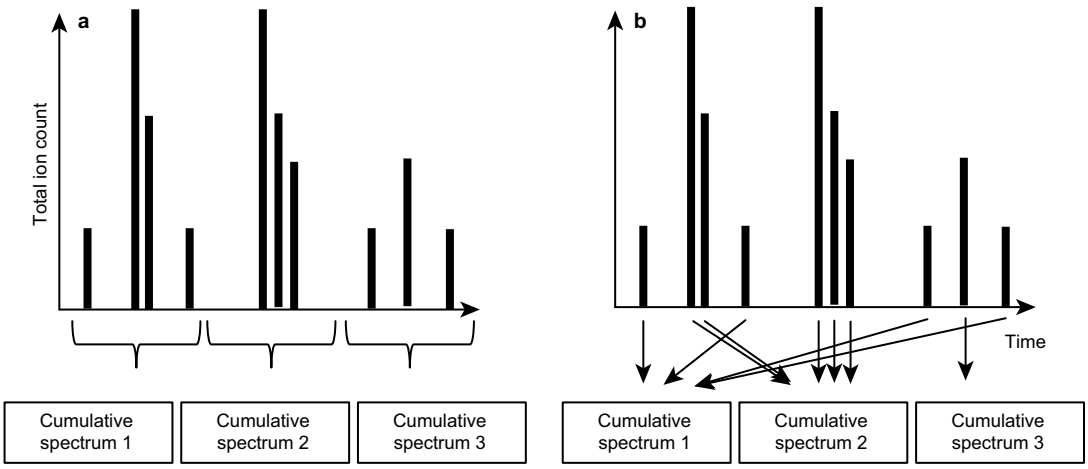

Fig. 2. Schematics of reconstructing spectrum in (**a**) traditional time-binning manner, and (**b**) method used in this work.

for each individual ion burst, (4) finding a background signal from the time series of TIC representing the background ion population, and (5) co-adding mass spectra signal that corresponds to the background.

Here, we need to separate the background signal from the signal that corresponds to ionization events. To obtain the background cumulative spectrum, let us mark a raw spectrum with no counts as "0" and spectrum that has counts

as "1". Now a raw spectrum that has an empty spectrum before and after is marked as "010", two consecutive spectra with the empty spectra before and after is marked as "0110", and so on. The background cumulative spectrum was calculated by co-adding all the counts from the spectra of the form "010", "0110" and "01110". The vast majority of these spectra contained only a single count. During the 10-ms sampling period, 75%–80% of the acquired spectra had no single count.

The ion plumes were divided into three classes according to the maximum counts during the ion bursts; 2–7 counts, 8–19 counts and 20–50 counts. These values are the actual measured counts during one acquisition period. When the transmission of the mass spectrometer and inlet as well as the sampling flow are taken into account, these maximum ion counts correspond to atmospheric ion concentrations of 1.5×10^3–5.2×10^3 cm^{-3}, 6×10^3–14×10^3 cm^{-3} and 15×10^3–45×10^3 cm^{-3}, respectively. Note that these values are not total ion counts during the whole ion plume, but instead maximum counts acquired during the 10-ms data acquisition period (during which 0.13 cm^3 of air is being sampled).

Data were processed using a MatLab toolbox called *tofTools* (Junninen *et al*. 2010). The mass spectrometer and the software have been described and applied in several studies (e.g. Ehn *et al*. 2010, 2011, 2014, Junninen *et al*. 2010, Kirkby *et al*. 2011, Lehtipalo *et al*. 2011, Manninen *et al*. 2011, Kangasluoma *et al*. 2013, Kulmala *et al*. 2013, Schobesberger *et al*. 2013, Riccobono *et al*. 2014).

Results

Characteristics of the ion bursts

In typical applications of atmospheric ion measurements, the instruments are operated at sampling frequencies of 0.001–1 Hz, and an average ion concentration during the acquisition period is recorded. The time series obtained from this type of measurements gives an impression that ions are relatively homogeneously distributed within the sampled air. In reality this is not the case.

When we the increased sampling rate to 100 Hz, a continuous-looking time series of air ions became spiky, with periods in between the spikes having few or no counts per spectrum (Fig. 3). Here, by a "spike" we mean a sudden increase in ion counts in the time series of the measured total ion concentration. Actually, each spike in the data is associated with one ionization event caused by a single ionizing interaction.

Typically, spikes with single counts were observed 13 to 14 times per second (Table 1). The frequency of spikes decreased rapidly with an increasing number of ion counts, so that the spikes with more than three ion counts were observed with frequencies of 1 Hz or less (Table 1). However, the exact frequencies have a minor importance by themselves, as they are dependent on the geometry of the ionization chamber. The used ionization chamber has a shape of a cylinder, so the effective ionization volume depends on the angle of incidence and radial position of the rays entering the chamber. The material of the chamber (stainless steel in this experiment) influences also the penetration of high-energy particles. The ionization events from the radon decay, however, are independent of the chamber material. The current system is not designed to replace or even to be used as a radiation detector. Still, if counting all the spikes regardless of the size as an event and comparing these frequencies with a laboratory radiation safety monitor (Berthold LB124), the obtained frequencies were in the same range, 9–20 Hz cm^{-2} (normalized to the projection area

Table 1. Frequency (Hz) of spikes grouped by counts in the spectrum. The projection area of the ionization chamber is 160 cm^2.

Counts of ions in the raw spectrum	Frequency at the flow of		
	2.8 l min^{-1}	8.8 l min^{-1}	16.8 l min^{-1}
1	14.5703	14.3933	13.4643
2	6.7592	4.8471	3.6098
3	1.8038	1.0811	0.6624
4	0.5416	0.2333	0.1583
5	0.2604	0.1104	0.0729
6	0.1708	0.0542	0.0437
7	0.1396	0.0437	0.0354
8	0.0750	0.0333	0.0354
9	0.0771	0.0396	0.0312
≥ 10	0.8290	0.5291	0.4103
> 0	24.8581	21.1546	18.4051

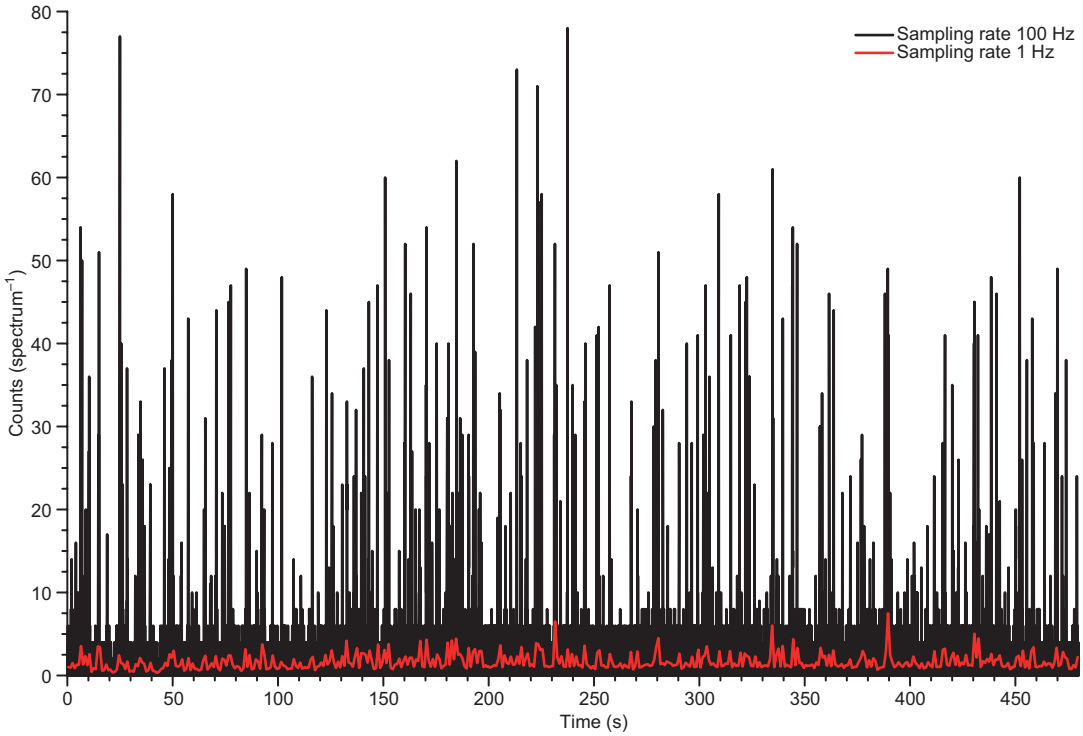

Fig. 3. Total ion count measured at two sampling rates, 100 Hz (black) and 1 Hz (red). The 1-Hz data were calculated by averaging from the 100-Hz data. Each spike corresponds to an ionization event taken place inside the continuous flow ionization chamber.

of ionization chamber). This indicates that the observed ion bursts were produced by cosmic rays along with α-, β- and γ-radiation.

The spikes in the time series of the total ion count (TIC) signal (Fig. 3) are formed when a cosmic ray or ionizing particle forms a plume of ions during the flight through the ionization chamber. We may assume that large (when multiple ions are detected) ion plumes originate from ionization events that are detected sooner after the event compared with the small plumes. This reasoning has multiple shortcomings, and the actual age of the ion plume cannot be calculated accurately. Other factors that affect the size of the plume are the angle of incidence and radial position of the ray as well as the type and energy of ionizing radiation in question. On average, however, the size of a plume is approximately related to its age. After the initial formation of the ion plume, ion–ion recombination starts to neutralize ions (Biondi 1969, Kontkanen *et al*. 2013), which lowers their total concentration. The carrier gas in the ionization chamber transports these ions to the mass spectrometer. Higher flow rates correspond to shorter average residence times and, consequently, longer residence times tend to provide more time for ions to be neutralized by the ion–ion recombination (*see* Table 1). Besides the ion–ion recombination, the ion plume is affected by diffusion broadening that makes the observed spikes wider. Again, with longer residence times, the observed spikes get wider.

In order to illustrate the effect of ion–ion recombination and diffusional broadening, a simplified and idealized one-dimensional model was constructed, in which the projection of the ion plume concentration to one dimension was assumed to follow a Gaussian distribution and any flow imperfections and wall losses were ignored. This is a valid assumption in a cases where the ionization takes place at the centre of the ionization chamber. The diffusion broadening was incorporated into the model by calculat-

ing the standard deviation of the Gaussian distribution shaped ion plume using the following equation:

$$\sigma = \frac{\sqrt{2Dt}}{\sqrt{2\log(2)}}, \quad (1)$$

where D is the diffusion coefficient and t is the time from the ionization event.

Figure 4 demonstrates the evolution of the moving (aging) ion plume. The initial ion concentration was set to 10^5 cm^{-3} in these calculations, and the values of D and ion–ion recombination coefficient were assumed to be 0.1 cm^2 s^{-1} and 8×10^{-7} cm^3 s^{-1}, respectively (Biondi 1969). Franchin *et al*. (2015) showed that the ion–ion recombination coefficient varies with temperature and humidity, but this variation was not taken into account here as our results are not very sensitive to the exact value of this parameter. This exemplary simulation on the evolution of the ion plume demonstrated that a faster moving carrier gas transports an ion plume more rapidly to the detector, leaving less time for the diffusion to broaden the spikes. Consequently, the plumes with the same age are different in height when using different carrier gas flow speeds.

In order to illustrate our findings further, the average properties of the spikes with different flow rates were calculated (using only spikes with total ion counts larger than 15). The analysis revealed that slightly higher frequency of the widest spikes occurred at lower carrier gas flow rates, and on average somewhat wider spikes were observed for positive ions (Fig. 5). The same was apparent when the median spikes were calculated separately for smaller (older) and large (younger) spikes. The reason for the wider spikes in the positive polarity is not clear. The spikes of the positive ions are not only wider but also they have much longer tail with all of the carrier gas flows (Fig. 6). This should be examined in more detail in subsequent studies.

Chemical composition of the ion plume and its evolution during the bursts

Our experimental system did not detect primary ions (N_2^+, O_2^- and e^-) because they have already transferred their charge to secondary ions by the time the ion plume reaches the mass spectrometer. The chemical composition of an ion plume at any given moment is defined by the concentration, proton or electron affinities and clustering ability of the substances present in the plume and carrier gas. After multiple sequential collisions, the composition of negative ions will be dominated by strong acids (proton transfer) or clusters of most abundant acids (Smith and Spanel 1996), just like in the case of atmospheric ions (Ehn *et al*. 2010). The time evolution of the acid equilibrium was nicely visible in our measurements (Fig. 7). The cumulative spectrum of the youngest ions plumes (Fig. 6d) was dominated by lactic acid (a mass-to-charge ratio (m/z) of 89.02 Th and the logarithm of the acid dissociation constant (pK_a) of 3.86) and nitric acid (m/z = 61.99 Th, pK_a = –1.4). When the plumes got older (Fig. 6b and c), the contribution of lactic acid decreased and that of sulfuric acid (m/z = 96.96 Th, pK_{a1} = –3, pK_{a2} = 1.99) increased. Finally, in the background spectrum (Fig. 6a), even the sulphuric acid dimer (m/z = 194.93 Th) became visible (Fig. 8). Another remarkable observation was that peaks in high masses appeared in the older plumes (Fig. 7a and b). There were groups of peaks starting from masses 344, 510, 676, 842 and 1008 Th with a separation of 166 Th, which could corresponds to the fragment C_3F_6O. The peaks in each group were separated by 16–18 Th, indicating molecular variations in the oxygen or water content. Most likely these high masses originated from impurities in the PTFE tubing, present in the lab air and in the tubing as a contamination.

The evolution of the chemical composition was also observed with the positive ions (Fig. 8), for which the young and old ion plume spectra were distinctively different, particularly in the masses higher than 250 Th. The lighter masses include NO^+ (m/z = 30.0 Th), $(H_2O)_2H^+$ (m/z = 37.03 Th), $C_3H_9O_3N^+$ (m/z = 107.06 Th) and $C_7H_{10}NO^+$ (m/z = 124.08 Th). The heavier masses at 536, 610, 684 and 758 Th had a separation of 74 Th that could be caused by CH_2SiO_2, and the whole series might originate from silicone tubing contaminations. All the heavier masses in the younger ion plumes (Fig. 9b–d) had a small positive mass defect (md; difference between the exact mass and integer mass),

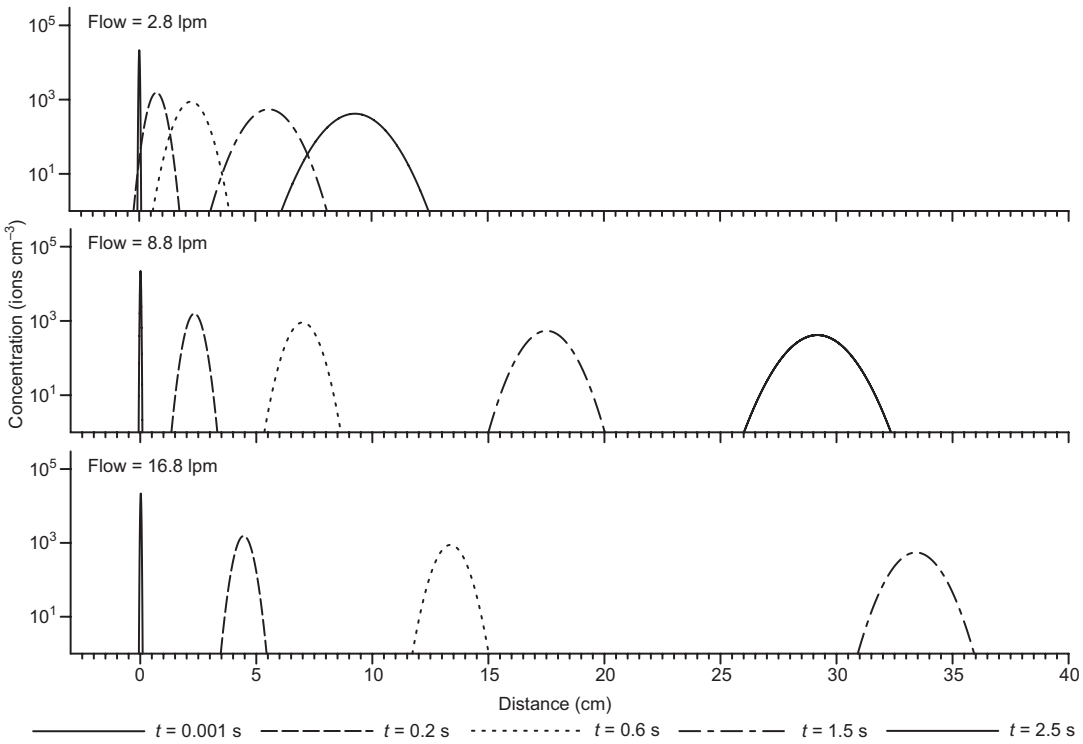

Fig. 4. Simulated evolution of an ion plume in a moving carrier gas. An ionization event is assumed to take place at the distance of 0 cm and the airflow in ionization chamber moves the plume towards the detecting instrument located at distance 40 cm.

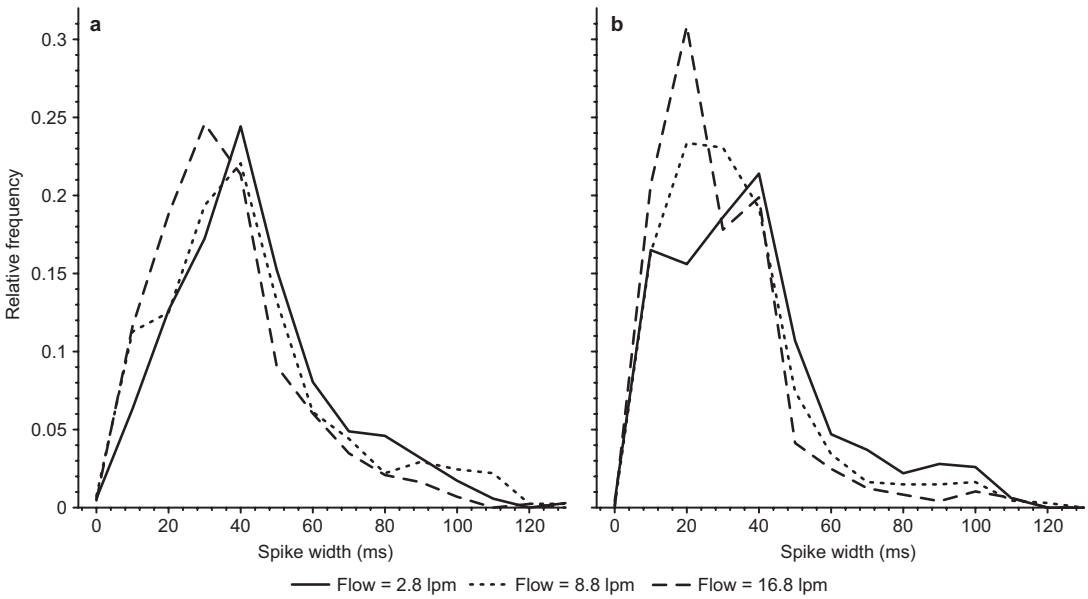

Fig. 5. Relative frequency distributions of widths of the ion bursts (full width at half maximum) for (**a**) positive ions and (**b**) negative ions.

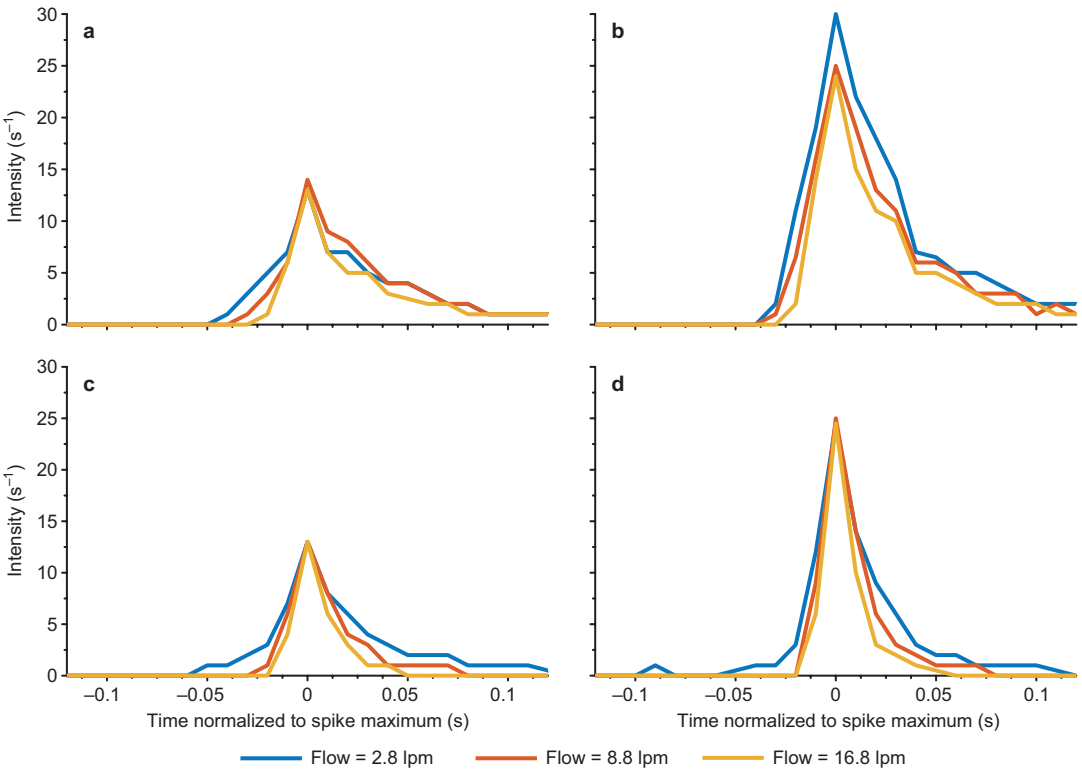

Fig. 6. Average (median) shapes of ion bursts for different carrier gas flow rates in the ionization chamber: (**a** and **b**) positive ions, (**c** and **d**) negative ions. In **a** and **c**, only bursts with maximum ion intensities between 8–19 were included for calculations; in **b** and **d**, the bursts with intensities of 20–60 [s^{-1}].

indicating that they must contain an element with a negative mass defect, such as *F* (m/z = 18.998 Th, md = –0.002) or Si (m/z = 27.977 Th, md = –0.032), to compensate for the positive mass defect of *H* (m/z = 1.008 Th, md = 0.0078). The group of ions appearing in the background spectrum between 200 and 500 Th had clearly a positive mass defect and patterns separated by 14–16 Th. This feature points to hydrocarbons. Even though the exact molecular identity and origin of the ion composition was not resolved, the power of our method to analyse chemical composition of short ion burst generated by high energy particles was clearly demonstrated.

This experiment was conducted using "dirty" laboratory air and the chemical speciation that was observed is specific for this experiment and necessary has no wider application. However, the observations of the existence of ion plumes that are high in concentration, but short in lifetime and spatial distribution, as well as the technology described to detect them, have wide applications, for example, to resolving the initial steps in the rapid oxidation chemistry in flow tube experiments or to quantifying the parameters affecting the ion dynamics.

Conclusions

We demonstrated the power of advanced mass spectrometry to analyse the chemical composition of ions within short bursts that are generated by high-energy particles originating from cosmic rays or radioactive decay. These ionization events are a significant pathway for the formation of ions in the atmosphere. In atmospheric sciences, ion spectrometers have been traditionally operated at too low sampling frequencies for detecting short-lived ion plumes (e.g. Manninen *et al*. 2009a, 2009b). Such a low sampling frequency provides an average concen-

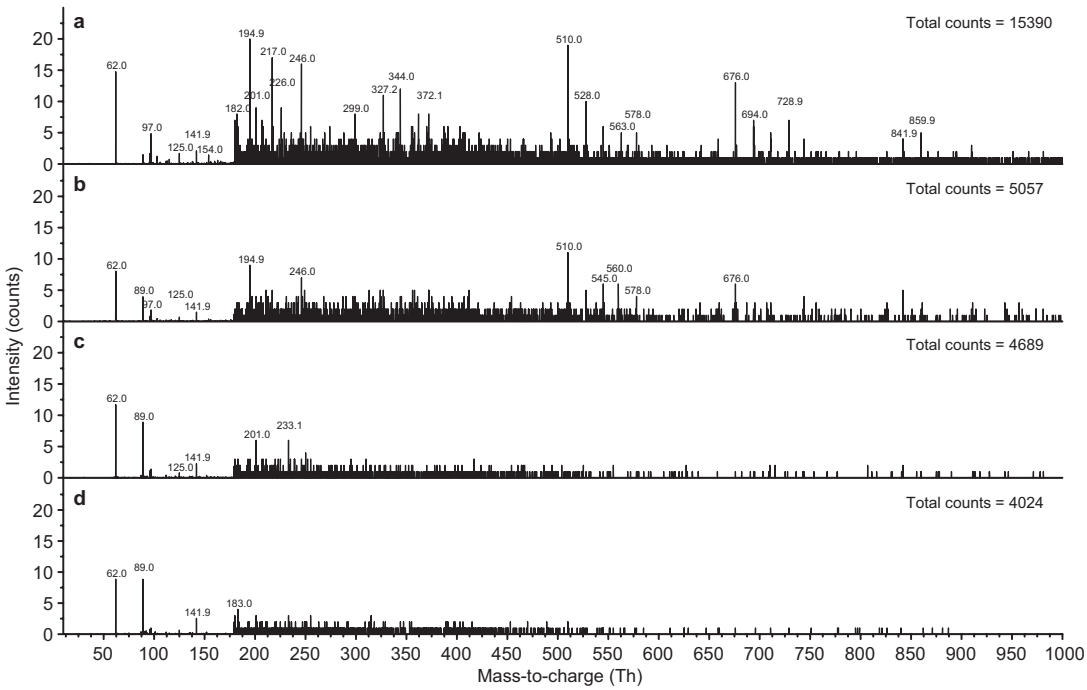

Fig. 7. Cumulative mass spectrum of observed negative ion bursts separated by the bursts intensity: (**a**) cumulative spectrum background, (**b**) sum of bursts that had maximum intensity of 2–8 counts, (**c**) sum of bursts with maximum intensity of 8–20 counts, and (**d**) sum of bursts with maximum intensity of 20–50 counts. The time from the initial ionization decreases from **a** to **d**. The value of total counts indicates the total number of counts summed up for each cumulative spectrum. Intensities for masses smaller than 180 Th were divided by 20.

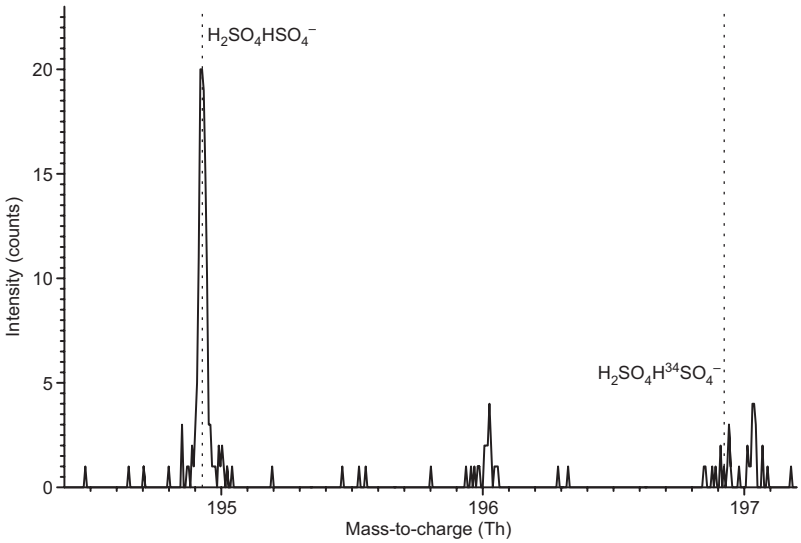

Fig. 8. Excerpt from the cumulative spectrum of background signal in Fig. 6a in order to provide a closer look at the correct identification of sulphuric acid dimer signal.

tration, which gives false image of a true spatial and temporal distributions of ions. Ions are not equally distributed, but instead there are regions with very high concentrations, and in majority of space and time there are no or few ions present.

By operating the mass spectrometer (APi-TOF) at the 100-Hz sampling frequency, we were able to detect ion plumes, to separate them from the background signal, to categorize them according to the ion density, and to

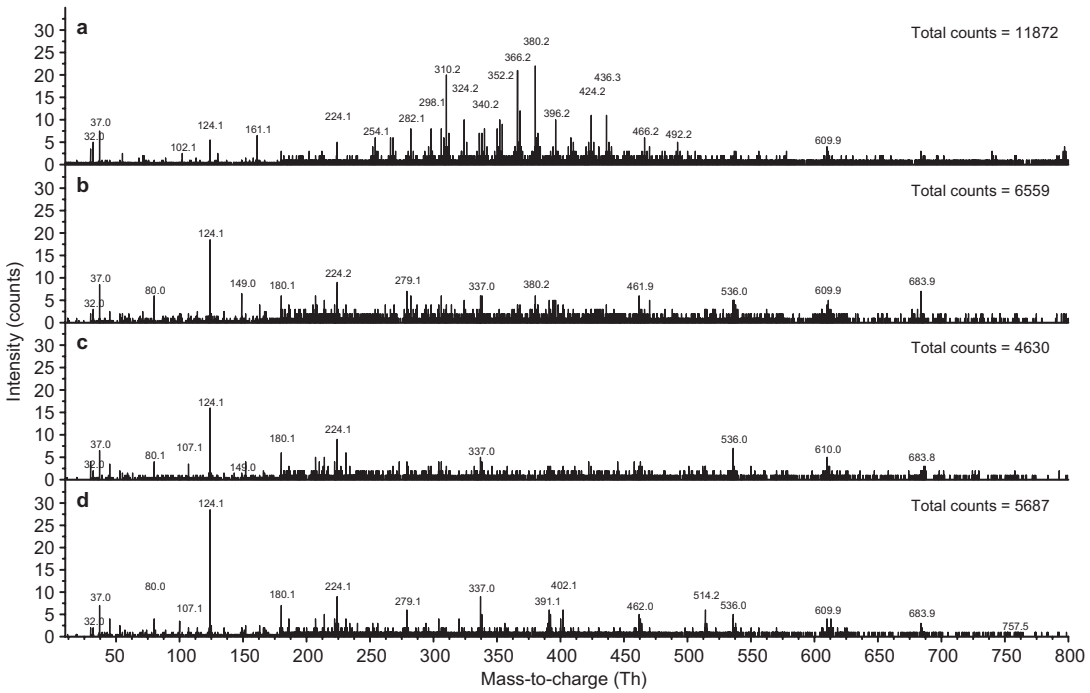

Fig. 9. Cumulative mass spectrum of observed positive ion bursts separated by the bursts intensity: (**a**) Cumulative spectrum of background, (**b**) sum of bursts that had maximum intensity of 2–8 counts, (**c**) sum of bursts with maximum intensity of 8–20 counts, and (**d**) sum of bursts with maximum intensity of 20–50 counts. The time from the initial ionization decreases from **a** to **d**. The value of total counts indicates the total number of counts summed up for each cumulative spectrum. Masses smaller than 180 are divided by 2.

measure their chemical composition. We could observe a clear change in the chemical composition of ion plumes as they aged. A distinct chemical composition was observed in young and old ion plumes for both negative and positive ions. Compared with negative ion plumes, the positive ion plumes tended to be spread to a larger volume while being lower in concentration.

The new setup provided direct information on individual ion bursts in an ambient air, including their "age" and the chemical composition of ions within such bursts. In general, the developed setup will provide new insight into the dynamics of ions and their chemistry. Such information is essential for detailed investigations on atmospheric oxidation, cluster dynamics, new-particle formation and gas-to-particle conversion.

Acknowledgements: We thank the Nordic Centre of Excellence CRAICC (no. 26060), Academy of Finland Centre of Excellence ATMNUCLE (grant no. 272041) and FP7-European Research Council — Advanced Grant project (project reference 227463) for financial support. We also thank the tofTools team for providing tools for mass spectrometry analysis.

References

Arnold F. 2006. Atmospheric aerosol and cloud condensation nuclei formation: a possible influence of cosmic rays? *Space Sci. Rev.* 125: 169–186.

Bazilevskaya G.A., Usoskin I.G., Fluckiger E.O., Harrison R.G., Desorgher L., Butikofer R., Krainev M.B., Makhmutov V.S., Stozhkov Y.I., Svirzhevskaya A.K., Svirzhevsky N.S. & Kovaltsov G.A. 2008. Cosmic ray induced ion production in the atmosphere. *Space Sci. Rev.* 137:149–173.

Calisto M., Usoskin I., Rozanov E. & Peter T. 2011. Influence of Galactic Cosmic Rays on atmospheric composition and dynamics. *Atmos. Chem. Phys.* 11: 4547–4556.

Das Gupta N.N. & Ghosh S. 1946. A report on the Wilson Cloud Chamber and its applications in physics. *Rev. Mod. Phys.* 18: 225–290.

Dickinson R. 1975. Solar variability and the lower atmosphere. *Bull. Am. Meteor. Soc.* 56: 1240–1248.

Duplissy J., Merikanto J., Franchin A., Tsagkogeorgas G.,

Kangasluoma J., Wimmer D., Vuollekoski H., Schobesberger S., Lehtipalo K., Flagan R.C., Brus D., Donahue N.M., Vehkämäki H., Almeida J., Amorim A., Barmet P., Bianchi F., Breitenlechner M., Dunne E.M., Guida R., Henschel H., Junninen H., Kirkby J., Kürten A., Kupc A., Määttänen A., Makhmutov V., Mathot S. , Nieminen T., Onnela A., Praplan A.P., Riccobono F., Rondo L., Steiner G., Tome A., Walther H., Baltensperger U., Carslaw K.S., Dommen J., Hansel A., Petäjä T., Sipilä M., Stratmann F., Vrtala A., Wagner P.E., Worsnop D.R., Curtius J. & Kulmala M. 2016. Effect of ions on sulfuric acid-water binary particle formation: 2. Experimental data and comparison with QC-normalized classical nucleation theory. *J. Geophys. Res. Atmos.* 121: 1752–1775.

Ehn M., Junninen H., Petäjä T., Kurten T., Kerminen V.-M., Schobesberger S., Manninen H.E., Ortega I.K., Vehkamäki H., Kulmala M. & Worsnop D.R. 2010. Composition and temporal behavior of ambient ions in the boreal forest. *Atmos. Chem. Phys.* 10: 8513–8530.

Ehn M., Junninen H., Schobesberger S., Manninen H.E., Franchin A., Sipilä M., Petäjä T., Kerminen V.-M., Tammet H., Mirme A., Mirme S., Horrak U., Kulmala M. & Worsnop D.R. 2011. An instrumental comparison of mobility and mass measurements of atmospheric small ions. *Aerosol Sci. Technol.* 45: 522–532.

Ehn M., Thornton J.A, Kleist E., Sipilä M., Junninen H., Pullinen I., Springer M., Rubach F., Tillmann R., Lee B., Lopez-Hilfiker F., Andres S., Acir I.-H., Rissanen M., Jokinen T., Schobesberger S., Kangasluoma J., Kontkanen J., Nieminen T., Kurtén T., Nielsen L.B., Jørgensen S., Kjaergaard H.G., Canagaratna M., Dal Maso M., Berndt T., Petäjä T., Wahner A., Kerminen V.-M., Kulmala M., Worsnop D.R., Wildt J. & Mentel T.F. 2014. A large source of low-volatility secondary organic aerosol. *Nature* 506: 476–479.

Eisele F.L. 1988. 1st Tandem Mass-Spectrometric measurement of tropospheric ions. *J. Geophys. Res.* 93: 716–724.

Flagan R.C. 1998. History of electrical aerosol measurements. *Aerosol Sci. Technol.* 29: 301–380.

Franchin A., Ehrhart S., Leppä J., Nieminen T., Gagné S., Schobesberger S., Wimmer D., Duplissy J., Riccobono F., Dunne E.M., Rondo L., Downard A., Bianchi F., Kupc A., Tsagkogeorgas G., Lehtipalo K., Manninen H.E., Almeida J., Amorim A., Wagner P.E., Hansel A., Kirkby J., Kürten A., Donahue N.M., Makhmutov V., Mathot S., Metzger A., Petäjä T., Schnitzhofer R., Sipilä M., Stozhkov Y., Tomé A., Kerminen V.-M., Carslaw K., Curtius J., Baltensperger U. & Kulmala M. 2015. Experimental investigation of ion–ion recombination under atmospheric conditions. *Atmos. Chem. Phys.* 15: 7203–7216.

Gagne S., Laakso L., Petäjä T., Kerminen V.-M. & Kulmala M. 2008. Analysis of one year of Ion-DMPS data from the SMEAR II station, Finland. *Tellus* 60B: 318–329.

Harrison R.G. & Ambaum M.H.P. 2008. Enhancement of cloud formation by droplet charging. *Proc. R. Soc. A* 464: 2561–2573.

Harrison R.G., Nicoll K., Takahashi Y. & Yair Y. 2015. Focus on high energy particles and atmospheric processes. *Environ. Res. Lett.* 10, 100201, doi:10.1088/1748-9326/10/10/100201.

Hirsikko A., Nieminen T., Gagné S., Lehtipalo K., Manninen H.E., Ehn M., Hõrrak U., Kerminen V.-M., Laakso L., McMurry P.H., Mirme A., Mirme S., Petäjä T., Tammet H., Vakkari V., Vana M. & Kulmala M. 2011. Atmospheric ions and nucleation: a review of observations. *Atmos. Chem. Phys.* 11: 767–798.

Iida K., Stolzenburg M., McMurry P.H., Dunn M.J., Smith J.N., Eisele F. & Keady P. 2006. Contribution of ion-induced nucleation to new particle formation: Methodology and its application to atmospheric observations in Boulder, Colorado. *J. Geophys. Res.* 111, D23201, doi:10.1029/2006JD007167.

Israël H. 1970. *Atmospheric electricity*, vol. I. Israel Program for Sci. Transl. & NSF, Jerusalem.

Junninen H., Ehn M., Petäjä T., Luosujärvi L., Kotiaho T., Kostiainen R., Rohner U., Gonin M., Fuhrer K., Kulmala M. & Worsnop D.R. 2010. A high-resolution mass spectrometer to measure atmospheric ion composition. *Atmos. Meas. Tech.* 3: 1039–1053.

Kangasluoma J., Junninen H., Lehtipalo K. Mikkilä J., Vanhanen J., Attoui M., Sipilä M., Worsnop D., Kulmala M. & Petäjä T. 2013. Remarks on ion generation for CPC detection efficiency studies in sub 3 nm size range. *Aerosol Sci. Technol.* 5: 556–563.

Kazil J. & Lovejoy E.R. 2004. Tropospheric ionization and aerosol production: A model study. *J. Geophys. Res.* 109, D19206, doi:10.1029/2004JD004852.

Kazil J., Zhang K., Stier P., Feichter J., Lohmann U. & O'Brien K. 2012. The present-day decadal solar cycle modulation of Earth's radiative forcing via charged H_2SO_4/H_2O aerosol nucleation. *Geophys. Res. Lett.* 39, L02805, doi:10.1029/2011GL050058.

Kirkby J., Curtius J., Almeida J., Dunne E., Duplissy J., Ehrhart S., Franchin A., Gagné S., Ickes L., Kürten A., Kupc A., Metzger A., Riccobono F., Rondo L., Schobesberger S., Tsagkogeorgas G., Wimmer D., Amorim A., Bianchi, F., Breitenlechner M., David A., Dommen J., Downard A., Ehn M., Flagan R.C., Haider S., Hansel A., Hauser D., Jud W., Junninen H., Kreissl F., Kvashin A., Laaksonen A., Lehtipalo K., Lima J., Lovejoy E.R., Makhmutov V., Mathot S., Mikkilä J., Minginette P., Mogo S., Nieminen T., Onnela A., Pereira P., Petäjä T., Schnitzhofer R., Seinfeld J.H., Sipilä M., Stozhkov Y., Stratmann F., Tomé A., Vanhanen J., Viisanen Y., Vrtala A., Wagner P.E., Walther H., Weingartner E., Wex H., Winkler P.M., Carslaw K.S., Worsnop D.R., Baltensperger U. & Kulmala M. 2011. Role of sulphuric acid, ammonia and galactic cosmic rays in atmospheric aerosol nucleation. *Nature* 476: 429–433.

Kontkanen J., Lehtinen K.E.J., Nieminen T., Manninen H.E., Lehtipalo K., Kerminen V.-M. & Kulmala M. 2013. Estimating the contribution of ion–ion recombination to sub-2 nm cluster concentrations from atmospheric measurements. *Atmos. Chem. Phys.* 13: 11391–11401.

Kulmala M., Riipinen I., Nieminen T., Hulkkonen M., Sogacheva L., Manninen H.E., Paasonen P., Petäjä T., Dal Maso M., Aalto P.P., Viljanen A., Usoskin I., Vainio R., Mirme S., Mirme A., Minikin A., Petzold A., Hõrrak

U., Plaß-Dülmer C., Birmili W. & Kerminen V.-M. 2010. Atmospheric data over a solar cycle: no connection between galactic cosmic rays and new particle formation. *Atmos. Chem. Phys.* 10: 1885–1898.

Kulmala M., Kontkanen J., Junninen H., Lehtipalo K., Manninen H.E., Nieminen T., Petäjä T., Sipilä M., Schobesberger S., Rantala P., Franchin A., Jokinen T., Järvinen E., Äijälä M., Kangasluoma J., Hakala J., Aalto P.P., Paasonen P., Mikkilä J., Vanhanen J., Aalto J., Hakola H., Makkonen U., Ruuskanen T., Mauldin R.L., Duplissy J., Vehkamäki H., Bäck J., Kortelainen A., Riipinen I., Kurten T., Johnston M.V., Smith J.N., Ehn M., Mentel T.F., Lehtinen K.E.J., Laaksonen A., Kerminen V.-M. & Worsnop D.R. 2013. Direct observation of atmospheric aerosol nucleation. *Science* 339: 943–946.

Laken B., Calogovic J., Shahbaz T. & Palle E. 2012. Examining a solar-climate link in diurnal temperature ranges. *J. Geophys. Res.* 117, D18112, doi:10.1029/2012JD017683.

Larin I.K. 2011. The effect of galactic cosmic rays on the chemical composition of the atmosphere, greenhouse effect and ozone layer of the Earth. *Russ. J. Gen. Chem.* 81: 2634–2640.

Lee B.P., Li Y.J., Flagan R.C., Lo C. & Chan C.K. 2013. Sizing characterization of the Fast-Mobility Particle Sizer (FMPS) against SMPS and HR-ToF-AMS. *Aerosol Sci. Technol.* 47: 1030–1037.

Lehtipalo K., Sipilä M., Junninen H., Ehn M., Berndt T., Kajos M.K., Worsnop D.R., Petäjä T. & Kulmala M. 2011. Observations of nano-CN in the nocturnal boreal forest. *Aerosol Sci. Technol.* 45: 499–509.

Manninen H.E., Nieminen T., Riipinen I., Yli-Juuti T., Gagne S., Asmi E., Aalto P.P., Petäjä T., Kerminen V.-M. & Kulmala M. 2009a. Charged and total particle formation and growth rates during EUCAARI 2007 campaign in Hyytiala. *Atmos. Chem. Phys.* 9: 4077–4089.

Manninen H.E., Petäjä T., Asmi E., Riipinen I., Nieminen,T., Mikkilä,J., Hõrrak U., Mirme A., Mirme S., Laakso L., Kerminen V.-M. & Kulmala M. 2009b. Long-term field measurements of charged and neutral clusters using Neutral cluster and Air Ion Spectrometer (NAIS). *Boreal Env. Res.* 14: 591–605.

Manninen H.E., Franchin A., Schobesberger S., Hirsikko A., Hakala J., Skromulis A., Kangasluoma J., Ehn M., Junninen H., Mirme A., Mirme S., Sipilä M., Petäjä T., Worsnop D.R. & Kulmala M. 2011. Characterisation of corona-generated ions used in a Neutral cluster and Air Ion Spectrometer (NAIS). *Atmos. Meas. Tech.* 4: 2767–2776.

Manninen H.E., Nieminen T., Asmi E., Gagné S., Häkkinen S., Lehtipalo K., Aalto P., Vana M., Mirme A., Mirme S., Hõrrak U., Plass-Dülmer C., Stange G., Kiss G., Hoffer A., Törő N., Moerman M., Henzing B., de Leeuw G., Brinkenberg M., Kouvarakis G.N., Bougiatioti A., Mihalopoulos N., O'Dowd C., Ceburnis D., Arneth A., Svenningsson B., Swietlicki E., Tarozzi,L., Decesari S., Facchini M.C., Birmili W., Sonntag A., Wiedensohler A., Boulon J., Sellegri K., Laj P., Gysel M., Bukowiecki N., Weingartner E., Wehrle G., Laaksonen A., Hamed A., Joutsensaari J., Petäjä T., Kerminen V.-M. & Kulmala M. 2010. EUCAARI ion spectrometer measurements at 12 European sites — analysis of new particle formation events. *Atmos. Chem. Phys.* 10: 7907–7927.

McMurry P.H. 2000. The history of CPCs. *Aerosol Sci. Technol.* 33: 297–322.

Mirme A., Tamm E., Mordas G., Vana M., Uin J., Mirme S., Bernotas T., Laakso L., Hirsikko A. & Kulmala M. 2007. Wide-range multi-channel Air Ion Spectrometer. *Boreal Env. Res.* 12: 247–264.

Mirme S. & Mirme A. 2013. The mathematical principles and design of the NAIS — a spectrometer for the measurement of cluster ion and nanometer aerosol size distributions. *Atmos. Meas. Tech.* 6: 1061–1071.

Mirme S., Mirme A., Minikin A., Petzold A., Hõrrak U., Kerminen V.-M. & Kulmala M. 2010. Atmospheric sub-3 nm particles at high altitudes. *Atmos. Chem. Phys.* 10: 437–451.

Mironova I.A., Aplin K.I., Arnold F., Bazilevskaya G.A., Harrison R.G., Krivolutsky A.A., Nicoll K.A., Rozonov E.V., Turunen E. & Usoskin I.G. 2015. Energetic particle influence on the Earth's atmosphere. *Space Sci. Rev.* 194: 1–96.

Pierce J.R. & Adams P.J. 2009. Can cosmic rays affect cloud condensation nuclei by altering new particle formation rates? *Geophys. Res. Lett.* 36, L09820, doi:10.1029/2009GL037946.

Porter H.S., Jackman C.H. & Green A.E.S. 1976. Apportionment of relativistic electron and proton energy among accessible modes in air. *Bull. Am. Phys. Soc.* 21: 358–358.

Raes F., Janssens A. & Van Dingenen R. 1986. The role of ion-induced aerosol formation in the lower atmosphere. *J. Aerosol Sci.* 17: 466–470.

Riccobono F., Schobesberger S., Scott C.E., Dommen J., Ortega I.K., Rondo L., Almeida J., Amorim A., Bianchi F., Breitenlechner M., David A., Downard A., Dunne E.M., Duplissy J., Ehrhart S., Flagan R.C., Franchin A., Hansel A., Junninen H., Kajos M., Keskinen H., Kupc A., Kürten A., Kvashin A.N., Laaksonen A., Lehtipalo K., Makhmutov V., Mathot S., Nieminen T., Onnela A., Petäjä T., Praplan A.P., Santos F.D., Schallhart S., Seinfeld J.H., Sipilä M., Spracklen D.V., Stozhkov Y., Stratmann F., Tomé A., Tsagkogeorgas G., Vaattovaara P., Viisanen Y., Vrtala A.,Wagner P.E.,Weingartner E., Wex H., Wimmer D., Carslaw K.S., Curtius J., Donahue N.M., Kirkby J., Kulmala M., Worsnop D.R. & Baltensperger U. 2014. Oxidation products of biogenic emissions contribute to nucleation of atmospheric particles. *Science* 344: 717–721.

Schobesberger S., Junninen H., Bianchi F., Lönn G., Ehn M., Lehtipalo K., Dommen J., Ehrhart S., Ortega I.K., Franchin A., Nieminen T., Riccobono F., Hutterli M., Duplissy J., Almeida J., Amorim A., Breitenlechner M., Downard A.J., Dunne E.M., Flagan R.C., Kajos M., Keskinen H., Kirkby J., Kupc A., Kürten A., Kurtén T., Laaksonen A., Mathot S., Onnela A., Praplan A.P., Rondo L., Santos F.D., Schallhart S., Schnitzhofer R., Sipilä M., Tomé A., Tsagkogeorgas G., Vehkamäki H., Wimmer D., Baltensperger U., Carslaw K.S., Curtius J., Hansel A., Petäjä T., Kulmala M., Donahue N.M. & Worsnop D.R. 2013. Molecular understanding of atmos-

pheric particle formation from sulfuric acid and large oxidized organic molecules. *Proc. Natl. Acad. Sci. USA* 110: 17223–17228.

Singh A.K., Siingh D. & Singh R.P. 2011. Impact of galactic cosmic rays on Earth's atmosphere and human health. *Atmos. Environ.* 45: 3806–3818.

Smith D. & Spanel P. 1996. Ions in the terrestrial atmosphere and in interstellar clouds. *Mass Spectr. Rev.* 14: 255–278.

Snow-Kropla E.J., Pierce J.R., Westervelt D.M. & Trivitayanurak W. 2011. Cosmic rays, aerosol formation and cloud-condensation nuclei: sensitivities to model uncertainties. *Atmos. Chem. Phys.* 11: 4001–4013.

Svensmark H. 1998. Influence of cosmic rays on Earth's climate. *Phys. Rev. Lett.* 81: 5027–5030.

Tammet H., Mirme A. & Tamm E. 2002. Electrical aerosol spectrometer of Tartu University. *Atmos. Res.* 62: 315–324.

Vana M., Ehn M., Petäjä T., Vuollekoski H., Aalto P., de Leeuw G., Ceburnis D., O'Dowd C.D. & Kulmala M. 2008. Characteristic features of air ions at Mace Head on the west coast of Ireland. *Atmos. Res.* 90: 278–286.

Voiculescu M. & Usoskin I. 2012. Persistent solar signatures in cloud cover: spatial and temporal analysis. *Environ. Res. Lett.* 7, 044004, doi:10.1088/1748-9326/7/4/044004.

Williams A.G., Zahorowski W., Chambers S., Griffiths A., Hacker J.M., Element A. & Werczynski S. 2011. The vertical distribution of radon in clear and cloudy daytime terrestrial boundary layers. *J. Atmos. Sci.* 68: 155–174.

Wilson C.T.R. 1899. On the condensation nuclei produced in gases by the action of röntgen rays, uranium rays, ultra-violet light, and other agents. *Phil. Trans. A* 192: 403–453.

Yu H. & Lee S.H. 2012. Chemical ionisation mass spectrometry for the measurement of atmospheric amines. *Environ. Chem.* 9: 190–201.

Zhang K., Feichter J.. Kazil J., Wan H., Zhuo W., Griffiths A.D., Sartorius H., Zahorowski W., Ramonet M., Schmidt M., Yver C., Neubert R.E.M. & Brunke E.G. 2011. Radon activity in the lower troposphere and its impact on ionization rate: a global estimate using different radon emissions. *Atmos. Chem. Phys.* 11: 7817–7838.